Reactor Hot Spot Analysis

by

Richard B. Vilim

Applied Physics Division
Argonne National Laboratory
9700 South Cass Avenue
Argonne, Illinois 60439

FRA TECHNICAL MEMORANDUM NO. 152

*Work supported by the U.S. Department of Energy.

Reactor Hot Spot Analysis

by

Richard B. Vilim

Applied Physics Division
Argonne National Laboratory
9700 South Cass Avenue
Argonne, Illinois 60439

FRA TECHNICAL MEMORANDUM NO. 152

*Work supported by the U.S. Department of Energy.

Reactor Hot Spot Analysis

by

Richard B. Vilim

Applied Physics Division
Argonne National Laboratory
Argonne, IL 60439

ABSTRACT

The principle methods for performing reactor hot spot analysis are reviewed and examined for potential use in the Applied Physics Division. The semistatistical horizontal method is recommended for future work and is now available as an option in the SE2-ANL core thermal hydraulic code. The semistatistical horizontal method is applied to a small LMR to illustrate the calculation of cladding midwall and fuel centerline hot spot temperatures. The example includes a listing of uncertainties, estimates for their magnitudes, computation of hot spot subfactor values and calculation of two sigma temperatures. A review of the uncertainties that affect liquid metal fast reactors is also presented. It was found that hot spot subfactor magnitudes are strongly dependent on the reactor design and therefore reactor specific details must be carefully studied.

*Work supported by the U.S. Department of Energy.

TABLE OF CONTENTS

TABLE OF CONTENTS (contd.)

TABLE OF CONTENTS (contd.)

LIST OF FIGURES

LIST OF TABLES

1. INTRODUCTION

Hot spot analyses are a standard part of core thermal hydraulic design and have been performed by the Applied Physics Division in support of several reactors. This report reviews the methods used in past Applied Physics work and presents some guidelines for future work.

The objective of this work is to survey existing hot spot methods, to review the requirements of the Applied Physics Division, to establish how hot spot analyses have been performed in the past in Applied Physics and to make recommendations as to what methods should be used in the future. This report defines the point from which future hot spot analyses should go forward.

This work is organized as follows. Section 2 gives a general description of uncertainties and their effect on core performance. Section 3 reviews the methods that are available for calculating how uncertainties affect peak core temperatures. Section 4 reviews what has been done in Applied Physics in the past, summarizes our requirements and makes a recommendation for a method to be used in the future. In Section 5 a discussion of the uncertainties that occur in the core and balance of plant is given. Finally, in Section 6 the recommended method is applied to a small LMR to illustrate calculation of two sigma peak cladding and fuel centerline temperatures.

2. BACKGROUND

2.1 Designing in the Presence of Uncertainties

One of the constraints faced by the reactor designer is that reactor conditions must not exceed design limits. These limits are chosen based on a knowledge of material properties and the requirement that structural integrity be maintained through life. For the core, full power limits are specified for assembly coolant exit temperature, cladding temperature and fuel centerline temperature.

It can be argued that operating limits can be approached very closely if the as built plant is an exact copy of the blueprint and if the analytic techniques used in modeling the plant are exact. This however neglects the fact that components are manufactured to finite tolerances and the models used in calculations often ignore second order effects. For example, approximations used in rod bowing models result in less than exact prediction of pin deformations with the result that subchannel flow areas input to a thermal hydraulic calculation will be in error. This then leads to a calculated subchannel temperature rise which is also in error. In practice then the as built plant will have process variable values that deviate from the design calculations. Therefore, if the design is set so that nominal variable values equal the design limits then some of these limits may be exceed in the as built plant as a result of the types of uncertainties discussed above.

To ensure proper and reliable operation, the designer must set nominal design values below the design limits so that there is sufficient margin in the presence of uncertainties. Two competing objectives must be balanced when setting the nominal operating conditions. Too large a margin between the nominal operating point and design limits penalizes reactor competitiveness while too small a margin may in the presence of uncertainties cause the limits to be exceeded and compromise fuel pin life and hence reactor performance.

Since the magnitude of uncertainties plays a major role in how closely the nominal design can approach the design limits, the treatment of uncertainties has received much attention. To express the degree to which actual reactor performance departs from the nominal design as a result of uncertainties, hot spot methods were developed. Their use has evolved since early application to light water reactor design in the 1950's.

2.2 Hot Spots

A standard set of hot spot includes cladding midwall temperature, fuel or absorber centerline temperature, assembly coolant exit temperature and gas plenum pressure. For each of these, the hot spot is located at the point where the variable takes on its maximum value. The effect of the uncertainties on the variable is included. Often a good approximation to the hot spot location is that point where the nominal value of the variable is a maximum. The location of the nominal maximum is dependent on the particular design and must be determined by analysis. Generally the maximum fuel centerline temperature will be at or slightly above the core midplane while the maximum cladding temperature will be near the top of the core.

The methods discussed below for computing hot spot values require that the variable be written in the sum format of Eq. 5. As it turns out, this is possible for all the core variables of interest. The expressions for cladding midwall and fuel centerline temperature are given below.

$$T_{\text{clad MW}} = T_{\text{in}} + \Delta T_{\text{coolant}} + \Delta T_{\text{film}} + \Delta T_{\text{clad MW}} \tag{1}$$

$$T_{\text{fuel CL}} = T_{\text{in}} + \Delta T_{\text{coolant}} + \Delta T_{\text{film}} + \Delta T_{\text{clad}} + \Delta T_{\text{gap}} + \Delta T_{\text{fuel}} \tag{2}$$

In addition, expressions can be written for assembly exit temperature and gas plenum pressure, as below. Since the use of Eqs. 3 and 4 in calculating hot spot quantities is almost identical to that for Eqs. 1 and 2, they are not pursued further in this work.

$$T_{\text{exit}} = T_{\text{in}} + \Delta T_{\text{coolant}} \tag{3}$$

$$P_{\text{plenum}} = \frac{nR}{V} T \tag{4}$$

where

n = number of moles of gas

R = universal gas constant

V = gas plenum volume

T = gas temperature

3. METHODS

Hot spot methods are an analytic means for representing the effect that modeling and manufacturing uncertainties have on the prediction of subassembly temperatures. The methods fall into two general groups, the hot rod approach and the probabilistic approach. In the hot rod approach the rod with the greatest nominal temperature, cladding or fuel centerline depending on the application, is selected and then the effect of uncertainties on the temperature at the hot spot for that rod is calculated. The resulting temperature is then compared with design limits to determine the design margin. If sufficient margin exists then all pins in the subassembly meet or better the design margin. In past LMFBR design work done in the U.S. (CRBR, FFTF), design limits have been specified for the hot rod so the hot rod approach has been used extensively[1]. In the probabilistic approach, the probability that each point in the core exceeds the design limit temperature is calculated. If the number of locations exceeding the design limit is less than a predetermined number then the design is adequate. In the rest of this report we focus on the hot rod approach since past U.S. LMFBR design limits have been stated in terms of temperature limits for the hot rod. The probabilistic methods are not considered further.

Development of the hot rod approach began with the Deterministic Method used in early light water reactors. This method proved to be too conservative with respect to as built temperatures. The result was excessively large margins between design limits and actual plant operating conditions. To overcome this problem the Statistical Method was developed and was first applied to the Enrico Fermi reactor. It however proved to be too optimistic with respect to as built temperatures. This led to the development of the Semistatistical Method, a hybrid of the Deterministic and Statistical methods. This method was adopted by Westinghouse for analysis of CRBR.

All three methods provide a means for determining the net effect on a core variable of the simultaneous occurrence of several uncertainties. The methods are applicable to any variable that can be written in the following analytic form

$$y = \sum_{i=1}^{m} F_i (x_1, \ldots x_n) \qquad (5)$$

where x_j = variable whose value is uncertain,

n = number of uncertain variables,

F_i = function of the uncertain variables

m = number of terms in the representation of y.

The above is the case for all hot spot variables of interest in core design, i.e. fuel and absorber centerline temperature, cladding temperature, coolant mixed mean exit temperature and gas plenum pressure for fuel, blanket and absorber assemblies.

Each hot spot method begins with the subfactor which expresses the effect of a single uncertainty on a single term in Eq. 5:

$$f_{ij} = \frac{F_i (\bar{\bar{x}}_1, \ldots \bar{x}_j + \Delta x_j, \ldots \bar{\bar{x}}_n)}{F_i (\bar{\bar{x}}_1, \ldots \bar{\bar{x}}_n)} , \tag{6}$$

where

$\bar{\bar{x}}_j$ = nominal value of x_j,

Δx_j = error in x_j relative to $\bar{\bar{x}}_j$.

If the uncertainty in x_j is a random variable then Δx_j is defined as one standard deviation. If the uncertainty is deterministic then Δx_j is the bias error in x_j.

3.1 Deterministic Method

The deterministic method assumes all uncertainties occur with their most unfavorable values at the same location and at the same time. The location is that of peak nominal conditions. Then from Eqs. 5 and 6 it is apparent that the hot spot value is approximately,

$$y = \sum_{i=1}^{m} \prod_{j=1}^{n} f_{ij} F_i (\bar{\bar{x}}_1, \ldots \bar{\bar{x}}_n) \tag{7}$$

This method is appropriate for representing errors whose magnitudes remain constant in time and space and can be estimated a priori. Examples include inlet flow maldistribution bias, cladding temperature increase beneath the wire wrap and biases introduced through reactor physics methods. The method has the disadvantage that reactor core uncertainties that have a statistical distribution of possible values, and hence do not always assume their worst case values, are not properly represented. This method tends to give results that are unnecessarily conservative with respect to the as built values.

3.2 Statistical Method

The probability that all the uncertainties take on their most unfavorable values at the same location at the same time is very small. This fact led to the development of the statistical method. In it each uncertainty is assumed to be a normal random variable with known standard deviation and a mean value of zero. The uncertainties are assumed to be independent. If the uncertainties are small in magnitude, then the two sigma bound on the hot spot is given by the "sum of squares" formulation:

$$y^{2\sigma} = \sum_{i=1}^{m} F_i (\bar{\bar{x}}_1, \ldots \bar{\bar{x}}_n) + 2 \left[\sum_{j=1}^{n} \sum_{i=1}^{m} (f_{ij} - 1) F_i (\bar{\bar{x}}_1, \ldots \bar{\bar{x}}_n)^2 \right]^{1/2} \tag{8}$$

where

f_{ij} = subfactor based on one standard deviation of uncertainty.

A two sigma variation is typically utilized as a figure of merit. Based on a normal distribution, the probability that the two sigma bound will not be exceeded is 97.7%. If the number of uncertainties is large, then this result is approximately valid even if the individual uncertainties have distributions other than normal. Examples of uncertainties that are well represented through the statistical method include manufacturing variability of fuel pellet fissile material content, dimensional tolerances and experimental uncertainties in correlations. The statistical method has the disadvantage that some errors are correlated and so the assumption of independence may not be valid. Further, certain errors are decidedly not statistical, rather they are known biases which should not be treated statistically.

3.3 Semistatistical Method

This approach is a hybrid of the above two and gives the designer the flexibility of specifying whether an uncertainty occurs as a constant bias or whether it assumes a statistical distribution of values. However to apply it meaningfully, one must justify the particular choice for each uncertainty, and this may not always be clear. The semistatistical method, as in the statistical method, is normally utilized to yield a two sigma bound.

There are four different expressions for the two sigma estimate. The basic expression is the "sum of squares" form and as is shown in Appendix A, it is derivable from first principles. The other three forms are all obtained from the sum of squares form by introducing a different mathematical inequality to evaluate it. Each inequality leads to a form that overestimates the two sigma value relative to the sum of squares form. Ranked with respect to the size of the two sigma value, the various forms from smallest to largest are sum of squares, horizontal, vertical and vertical heat flux* Appendix A gives a proof of the ranking.

The four approaches have the following historical significance. The sum of squares form although it is the basis for the others does not appear to have been used in design work. The reason for this is not clear. The horizontal form was used in more recent CRBR work (Ref. 2) while the vertical form was used in the earlier work (Ref. 3). Reference 1 states that the vertical form "was conservatively adopted for convenience in calculation and to provide additional margin in the early stages of design" while the horizontal form "is more exact, and is being used for future analyses". The vertical heat flux form was used in Reference 3. It differs from the vertical form only in that local heat flux subfactors are lumped together to form a separate heat flux hot channel factor instead of being lumped in with the more usual coolant, film and cladding hot channel factors. The mathematical specifics are given in Appendix A.

The semistatistical method of Appendix A must be extended before the effect of uncertainties in the balance of plant on core temperatures can be represented. The extension given in Appendix B is based on that developed for CRBR and given in Reference 2. It is based on the observation that all

---

*A variation of the vertical method, as described in Subsection A.6.

balance of plant uncertainties appear as perturbations in reactor inlet temperature and flowrate. Additionally these two quantities are not statistically independent but are correlated and as a result the assumption of independent errors made in Appendix A in the derivation of the semistatistical method is not valid. Obtaining values for the statistical parameters of Appendix B requires a Monte Carlo analysis of the plant of the type done in Reference 2.

4. SELECTION OF A METHOD

This section begins with a review of what the Applied Physics Division presently requires from a hot spot analysis. The suitability of the past approach to filling present needs is then assessed. Recommendations for a hot spot methodology are then given based on these findings.

The principle requirement is that the method be defensible. A candidate method must have a rigorous analytic basis, permit treatment of different error types, have been shown to give realistic temperature estimates and use data which can be determined based on measurements or estimates. Additionally the method should be amenable to computer solutions so that it can be used in routine design applications.

The main weakness of the method used in the past in the Applied Physics Division has been a lack of documentation. The method has been referred to as the "five factor" method since, as it is implemented in NIFD, five factors are input to the code to generate two sigma temperatures. This implementation was never documented and so the rationale for adopting it or its technical basis was never recorded. However, it appears this method is the vertical heat flux form described in Appendix A. Four of the five factors appear to be coolant, film, cladding and heat flux hot channel factors as defined in Appendix A. The meaning of the fifth factor is somewhat obscure. Past hot spot analyses done in the Division have used this method and taken numerical values for the first four of these factors from CRBR, specifically from the second to the last row of Table I of Ref. 3, and applied them to reactors other than CRBR. The application of CRBR data to other reactors was not necessarily appropriate in all cases. Clearly the past method is vague and is therefore difficult to defend.

A fresh approach to hot spot analysis done within the Applied Physics Division is warranted. With respect to the four selection criteria listed above there is one method that satisfies them. It is the horizontal version of the semistatistical method described in Appendix A. The method has a rigorous analytic basis and this is given in Appendix A. The method can handle both bias errors and random uncertainties. This method was selected for use in the later stages of CRBR core uncertainty analysis. Considerable effort was invested in demonstrating that the method gives good uncertainty prediction. It is unlikely that an effort equivalent to that done for CRBR could be mounted by Applied Physics. Finally, the uncertainty data required can be obtained by a combination of experiment and analysis. Therefore, the semistatistical horizontal method is recommended for use in future hot spot analyses.

5. UNCERTAINTIES

This section presents a discussion of the uncertainties associated with liquid metal fast reactor cores. For the most part, these uncertainties occur in any fast reactor that uses the hexagonal assembly with wire wrapped pins as the basic core building block.

Since conventional control assemblies consist of wire wrapped pins in a hex can, the uncertainties affecting a control assembly are almost identical to those found in a blanket or fuel assembly. Therefore no distinction is made in the discussion below between the various assembly types. A reference to an "assembly" applied equally to a fuel, blanket or control assembly.

In the discussion below, the uncertainties have been lumped according to their affect on a specific core variable. The variables discussed are reactor power level, reactor power distribution, reactor flowrate and inlet temperature, assembly flowrate and inlet temperature, subchannel coolant temperature rise and film and clad temperature rise.

5.1 Reactor Power Level

If an uncertainty exists in total reactor power under full power conditions, then pin and coolant temperatures may exceed their nominal design values. The error in reactor power level and its effect on core temperatures is represented through subfactors applied to the subchannel coolant temperature rise.

Measurement errors result in an uncertainty in reactor power level as follows. Steady state reactor power level is determined by measuring reactor coolant inlet temperature, outlet temperature and mass flowrate and then applying an energy balance to yield computed power. Error in the computed power however arises out of calibration errors in the temperature and flow sensors. The error in computed power ultimately appears as an uncertainty in actual reactor power since the reactor control system operates to set to zero the difference between demanded and computed power. If the computed power contains a bias error relative to the actual power, then the actual power will not equal the demanded power.

5.2 Reactor Power Distribution

Factors that may cause the calculated power distribution to differ from the actual are discussed below. The error in power distribution is represented through subfactors applied to subchannel coolant temperature rise and local heat flux.

5.2.1 Reactor Physics Model Uncertainty

Uncertainties associated with reactor physics models include those that arise out of modeling in fewer than three dimensions, those errors associated with predicting burnup, application of diffusion theory where not legitimately valid and interpolation of pin power from a neutronics grid that is not coincident with the subchannel grid.

5.2.2 Control Rod Banking Uncertainty

Control rods are typically grouped into a set or bank in which all the rods move as a unit. However, because of manufacturing tolerances, all the rods in a bank do not necessarily penetrate the same depth; when this is the case the power is perturbed locally in the area of the rod.

5.2.3 Fissile Fuel Distribution Uncertainty

Deviation in fissile content of a pellet from the design value perturbs the pellet power from the nominal. Since pellets are produced in batch it is possible that an entire fuel pin of pellets could have a similar error in fissile concentration.

5.2.4 Nuclear Data Uncertainty

Basic nuclear data such as fission cross sections, fission yields and gamma heating cross sections are all derived from experiment and thus may contain experimental error. Generally, nuclear data is not known to within one percent.

5.3 Reactor Flowrate and Inlet Temperature

The temperatures attained in an assembly are in part dependent on the core boundary conditions of inlet temperature and flowrate. Uncertainties in these boundary conditions are represented through subfactors which are applied to subchannel inlet temperature and subchannel temperature rise.

Perturbation of reactor flowrate and inlet temperature from their nominal values are induced by balance of plant uncertainties. Fouling of intermediate heat exchanger surfaces, if not adequately represented in the nominal design calculations, will result in a difference between nominal and observed core inlet temperature. Primary system frictional losses or pump characteristics, if in error, will induce an uncertainty in reactor mass flowrate.

5.4 Assembly Flowrate and Inlet Temperature

For the reasons described below the temperature and flowrate calculated for the inlet of an assembly may differ from the actual.

5.4.1 Loop Temperature Imbalance Uncertainty

In a multiloop plant, fluid from the cold legs mixes in the inlet plenum and is then distributed by the inlet modules to the core assemblies. Normally the cold legs are at the same temperature. However in some modes of operation, temperature differences between cold legs can exist. When this occurs, not all the flow modules will have the same temperature because of less than perfect mixing in the inlet plenum.

Depending on the analytic models used to describe the plenum mixing it may be necessary to introduce a hot spot factor to account for those modules having a coolant temperature higher than the average. Such a factor is required if design calculations failed to represent the three dimensional mixing as would be the case if a perfect mixing model were used.

In addition, often the geometry of the inlet plenum is so complex that it is almost impossible to obtain an accurate analytic description of fluid mixing and the distribution of inlet module temperatures. What is typically done in this case is to run a mixing experiment with loop temperatures set so that the largest credible temperature imbalance exists between loops. The deviation of the hottest inlet module temperature from the average is measured and this value is then used to compute a hot spot factor.

5.4.2 Interassembly Flow Distribution Uncertainty

Uncertainty in the flowrate calculated for each assembly is introduced by modeling errors, manufacturing tolerances and systematic error. Modeling errors include error implicit in component pressure drop correlations and error associated with representing complex multidimensional flow such as that found in the inlet plenum. Manufacturing tolerances introduce uncertainties in the exact dimensions of components such as orifice plates and flow distribution hardware. Obviously a precise knowledge of these dimensions is a necessary condition for their accurate hydraulic representation. Systematic error is error induced in one component as a result of errors in the calibration of another component. For example, incorrect blanket assembly flow resistance will result in a flow bias in fuel assemblies.

5.5 Subchannel Coolant Temperature Rise

Calculated subchannel temperatures may differ from those observed in the plant for any of the reasons discussed below.

5.5.1 Intraassembly Flow Distribution Uncertainty

Coolant flowrate and temperature distribution among subchannels within an assembly is normally calculated using a subchannel code such as SUPERENERGY-2 (Ref. 6). In these codes, empirical constants are an integral part of the models used to describe wire wrapped induced crossflow and turbulent mixing. Values for the constants are obtained by making thermal hydraulic measurements on a benchmark assembly and then adjusting the code constants so that the difference between measured and code calculated temperatures is minimized. However because of measurement errors and the inability of the mixing model to completely represent the velocities in a wire wrapped bundle, code generated temperatures cannot be fit exactly to measurement. The error is represented through hot spot subfactors applied to subchannel temperature rise and film temperature.

5.5.2 Subchannel Flow Area Uncertainty

Manufacturing tolerances in the construction of assemblies and modeling errors in the prediction of fuel pin bowing contribute to a subchannel flow area that deviates from the nominal design value. As a result the hydraulic characteristics of the subchannel differ from the nominal.

5.5.3 Wire Wrap Orientation Uncertainty

The flow and temperature distribution within an assembly depends slightly on the relative orientation of wire wraps and power skew. Since this effect is not accounted for in the subchannel codes used in the nominal analysis, it is a source of error.

5.5.4 Coolant Property Uncertainties

The specific heat and density of the coolant are used in the momentum and energy equations to determine coolant temperature in a subchannel. Since property correlations are obtained from experiment, they contain measurement errors.

5.6 Film and Cladding Temperature Rise

Uncertainties affecting the temperature rise across film and cladding are as follows.

5.6.1 Film Heat Transfer Coefficient Uncertainty

The application of a correlation that was derived from measurements performed in a particular assembly to an assembly of different dimensions and possibly different geometry is a potential source of error. Even though the correlation may be in a nondimensional form, it is still being applied outside the data base upon which it was derived. In addition measurement errors in the data on which the correlation is based contribute to the uncertainty.

5.6.2 Pellet Cladding Eccentricity Uncertainty

If a fuel pellet is not positioned concentrically within the cladding, then at some circumferential location the clad-pellet gap is less than the nominal value. Gap resistance at this location is reduced and hence the heat flux is increased. As a result, the cladding and film temperature rises are greater than nominal. However, since the gap closes with burnup, this effect is important only at beginning of life.

The effect of pellet-cladding eccentricity on fuel temperature is to lower the maximum temperature. This implies that the fuel subfactor is less than unity.

5.6.3 Cladding Circumferential Temperature Distribution Uncertainty

The distribution of coolant temperature and axial velocity around a fuel pin shows a strong azimuthal dependence. Consequently the cladding temperature also has a circumferential dependence. Hot spots within this distribution are further aggravated by the effects of the wire wrap.

In a calculation of assembly conditions with a subchannel code such as SUPERENERGY-2, the full circumferential distribution is not solved for, but instead an average temperature over a 60 degree sector is obtained. As a result the peak cladding temperature, which occurs at the point where the fluid gap is a minimum, is not available. A hot spot factor is used to obtain the peak value from the 60 degree average.

5.6.4 Cladding Conductivity and Thickness

Uncertainty in cladding conductance result from uncertainties in the cladding conductivity correlation and from irradiation induced changes in conductivity and thickness.

6. APPLICATION TO A SMALL LMR

To illustrate the semistatistical horizontal method, we use it below to calculate the fuel centerline and cladding hot spot temperatures for an arbitrary small LMR. This small reactor provides a wide range of interesting features to apply the hot spot analysis to.

6.1 Description

The small LMR chosen here is a 39 MWt fast reactor producing 10 MWe via a Brayton cycle. The primary system consists of a single loop NaK circuit driven by an EM pump and uses three NaK-gas heat exchangers that operate in parallel to transfer energy to the gas secondary side.

The core consists of nineteen fuel assemblies arranged in the form of a cylinder. There are no blanket assemblies. Control assemblies are also absent with control being achieved via six hinged exvessel reflectors that wrap around the outside of the core. At the end of life, reactivity is low enough that the reflectors are completely closed, forming an annulus around the core.

The fuel assembly is typical of a fast reactor. It consists of a hex can housing 217 wire wrapped fuel pins. The dimensions are given in Table I. Figure 1 shows a typical fast reactor fuel assembly and is representative of a small LMR design.

Some hot spot subfactors for this reactor can be extracted directly from CRBR work given the similarity between fuel assemblies for the two designs. Comparing via Table I shows that the two are similar with respect to their hex geometry, number of pins, fuel pin design, use of wire wraps and the duct flat-to-flat width.

Other hot spot subfactors such as those associated with the core power distribution will have appreciably different values. For example, this small LMR is chosen to be a homogeneous core and therefore is free from the abrupt material transitions found at blanket fuel assembly interfaces in heterogeneous cores. The neutronics at such interfaces cannot be modeled to the accuracy that homogeneous regions can and therefore are subject to greater uncertainty in local power. The absence of such interfaces in this example works to reduce the magnitude of the reactor physics hot spot subfactor compared to the CRBR homogeneous core.

Finally, the classification of uncertainties as direct or statistical follows exactly that of CRBR. In that work it appears that some uncertainties that could be considered deterministic were treated as statistical. One reason for this might be that such uncertainties rarely combine simultaneously so that their net effect is more accurately represented by treating each of them statistically.

6.2 Cladding Hot Spot

In this subsection, the cladding hot spot temperature is calculated using the methods recommended in this work. This involves first identifying the origin of uncertainties, determining their magnitudes, computing subfactor

TABLE I. Fuel Assembly Dimensions

	CRBR	Small LMR
Duct		
Geometry	hexagonal	hexagonal
Inner flat-to-flat, m	0.1101	0.1280
Wall thickness, m	3.05×10^{-3}	3.048×10^{-3}
Pin		
Number	217	217
P/D ratio	1.24	1.194
Outer diameter, m	5.842×10^{-3}	9.398×10^{-3}
Cladding thickness, m	3.81×10^{-4}	6.35×10^{-4}
Gap	1.65×10^{-4}	
Bond type	gas	He
Pellet density, % TD	91.3	91.3
Fuel length, m	0.914	1.98
Upper axial blanket length, m	0.356	0
Lower axial blanket length, m	0.356	0
Fission gas plenum length, m	1.219	1.98
Spacer		
Type	helical	helical
Pitch, m	0.3048	0.3048
Diameter, m	1.422×10^{-3}	1.626×10^{-3}
Volume Fractions		
Fuel and gap	0.347	0.3998
Structure	0.234	0.234
Sodium	0.419	0.3653

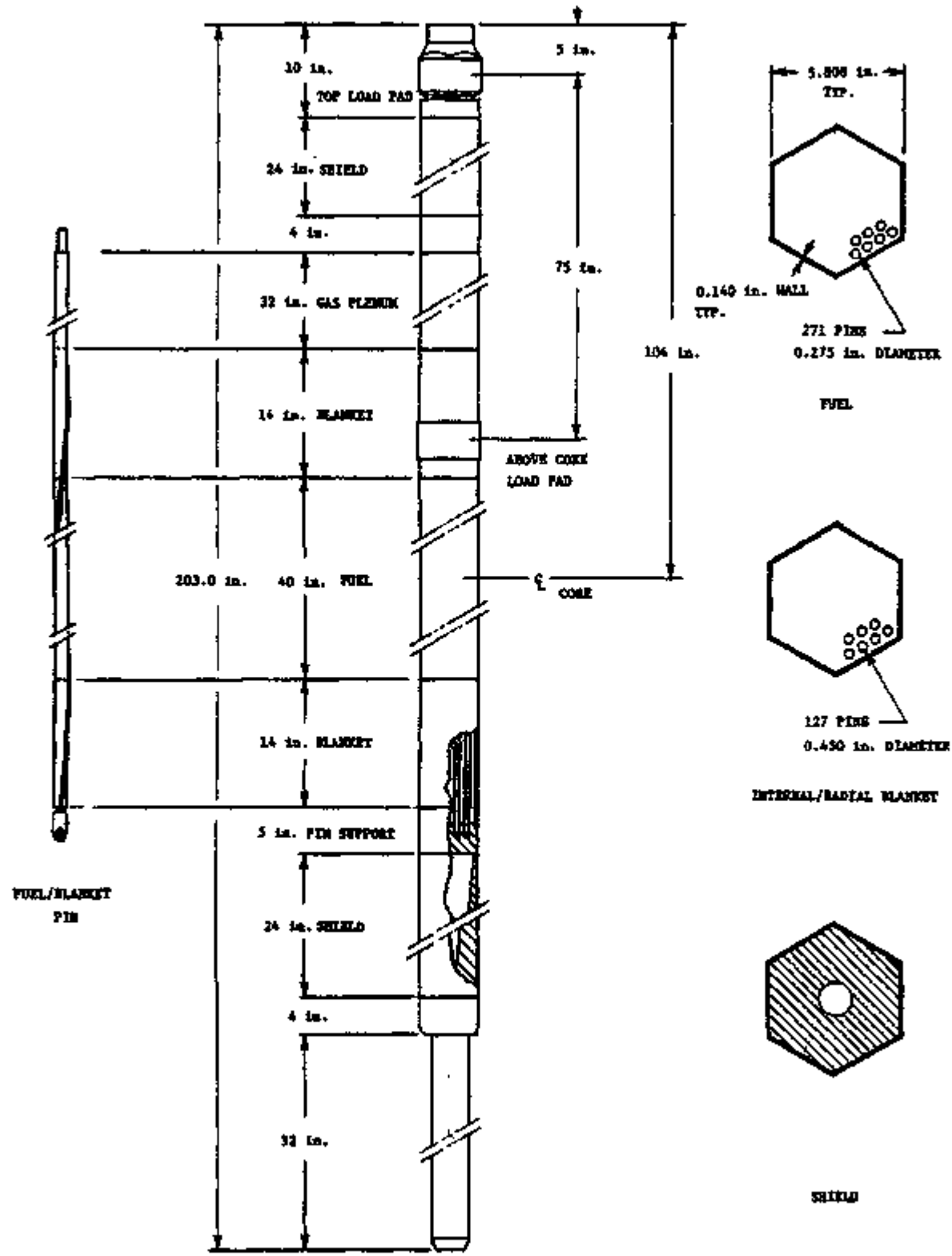

Fig. 1. Representative Fast Reactor Fuel Assembly

values and finally calculating a cladding two sigma temperature via the semistatistical horizontal approach. The value is then compared with that gotten in Ref. 4 which applied the methods of past AP hot spot analyses.

The location of the cladding hot spot will be taken from Ref. 4 where it was determined as follows. REBUS was run to produce power densities and these were then input to SUPERENERGY-2 to yield coolant temperature rises in each subchannel of the core. A hand calculation using data from the above runs produced nominal film and cladding temperature rises. The results showed that the peak nominal cladding temperature at BOL is reached at the top of the core in the center assembly.

6.2.1 Measurement Uncertainty

The magnitude of measurement errors and their treatment will be taken from the CRBR work. There the power control system measurement errors were lumped in with the balance of plant uncertainties, so the same is done here. See the Balance of Plant discussion below. Values for measurement error subfactors are therefore set to unity.

6.2.2 Reactor Physics Model Uncertainty

The modeling of the hinged reflectors presents the greatest source of uncertainty in the reactor physics calculations. Presently the neutronics are modeled using a two-dimensional RZ diffusion code that represents the reflector region by an annulus that surrounds the core. The number density of the annulus represents the degree of reflector closure. However, as yet the number densities used are not based on a rigorous homogenization scheme so they are only a rough estimate as to a 2-D representation.

This two-dimensional treatment of neutronics introduces errors as follows. First, at beginning of life, the six reflectors are open so that the reactor geometry is three dimensional with a 60 degree symmetry section. Although the reflector geometry has an azimuthal dependence, within this 60 degree sector, the r-z two-dimensional cylindrical representation will average out this dependence and obscure local power peaks. Second, there is some question as to how appropriate, for a particular reflector angular position and in the absence of proper homogenization, the number densities are for representing the reflector behavior. Third, diffusion theory is not strictly valid at the reflector core interface. If these three error sources are to be accurately quantified then a Monte Carlo simulation or critical experiment must be performed. For the present, estimates for the above errors will have to suffice.

Failure to use a 3-D calculation to represent reflector assymmetry should not be important at BOL since the peak subchannel is in the center assembly where azimuthal dependence is very small. As the burn cycle progresses to EOC, the peak subchannel moves out to the core periphery where at EOC the reflectors are completely closed and therefore the power shows no azimuthal dependence (except possibly from the uneven azimuthal burn at BOL). Hence the effect of doing the neutronics calculation in 2-D instead of 3-D should have only a small effect on peak subchannel temperature. A somewhat arbitrary error of 1% is assigned.

Next, for error introduced as a result of an improper reflector number density, we have the following. A separate calculation showed that perturbing the reflector number density from 60% to a value of 70% altered the midplane power by 5.7% at the core center and by 6.3% at the periphery. Therefore, if based on this result, we assume a somewhat arbitrary error of 5% in reflector number density, the peak subchannel power will be off by approximately 3%.

Finally, for errors introduced by using diffusion theory at the core-reflector interface, the error in peak subchannel power is estimated to be 1%. This is based on a statement in Ref. 5 that for 60 to 70 cm radius homogeneous cores with no control rods, calculated reaction rates differ from measured by less than 1% at most points in the core more than 5 cm from the blanket.

Another source of error lies in fitting power as calculated by the neutronics code to pin power input to the subchannel code. The neutronics nodalization is usually much coarser than the subchannel grid so that pin power must be interpolated from the neutronic nodes. The interpolation error for CRBR was determined to be 1%. For the small LMR it will be of similar magnitude but the exact value will depend on the neutronic mesh size and the type of interpolation scheme. A tentative value of 1% is used until the problem can be studied further.

The above uncertainties combine to an overall direct uncertainty of 6% which is applied to both integrated channel power and local heat flux. This number is treated as an estimate until an appropriate Monte Carlo simulation or experiment is carried out to obtain a more sound working value.

6.2.3 Control Rod Banking

The typical fast reactor control rods and assemblies are replaced in this example by a set of six hinged reflectors. Since these function to control reactivity, it is appropriate to consider the effect of an asymmetry in their position on local power. An accurate estimate of the maximum perturbation to local power by such an asymmetry is rather vague at this time for several reasons. First, the out-of-bank tolerances can only be estimated. Secondly, even if the tolerance was known, the Monte Carlo simulations required to quantify the impact would be prohibitively expensive. Therefore, an estimate of the error will have to suffice. Parametric calculations performed for CRBR showed that the maximum error in local power induced by control rod out-of-banking was 4% adjacent to a control rod and 2% otherwise. Since the effect of a single hinged reflector should be more spatially distributed than a control rod, a direct value of 2% will be used here.

6.2.4 Fissile Fuel Distribution

Since the same fuel pellet fabrication techniques as were proposed for CRBR are assumed, it is also reasonable to assume the CRBR hot spot values. There the uncertainty in subchannel temperature rise and in local heat flux due to fissile fuel content uncertainty was estimated to have a three sigma value of 5.2%.

6.2.5 Nuclear Data

Experiments performed on the ZPPR-7 critical assembly (Ref. 2) and on certain homogeneous cores (Ref. 5) provide a measure of the local power uncertainty that might be expected as a result of nuclear data uncertainty.

In the ZPPR-7 experiments, a heterogeneous core was mocked up using blanket and fuel assemblies. A comparison of measured fission and gamma reaction rates with calculations showed the three sigma uncertainty in power in the fuel to be 7%. This value was then used in the CRBR hot spot analysis to represent the uncertainty in power due to errors in nuclear data such as fission, capture and gamma heating rates. Assigning this error exclusively to nuclear data and then having a separate hot spot value for nuclear model errors may have been conservative since the 7% probably represents both data and methods error.

For clean (no control rods) homogeneous cores of 60-70 cm radius, the French computed reaction rate distributions to within 1% of experiment at most points in the core more than 5 cm from the blanket (Ref. 5). Again both reactor physics methods and nuclear data errors are present in this value.

These two sets of results probably bound the uncertainty in the small LMR calculated power. This core is homogeneous and at beginning of life has a uniform fuel enrichment. As the burn cycle progresses, the interior region depletes more rapidly than the periphery. But Ref. 5 indicates that errors in reaction rates increase as the difference in enrichment between adjacent regions increases. Thus using the homogeneous and the heterogeneous results above and interpolating for the interior depletion at end of life, the error in nuclear data is estimated to cause a three sigma uncertainty in local and channel integrated power of 2%.

6.2.6 Balance of Plant

An accounting of the effect of balance of plant uncertainties on the core inlet temperature and core flowrate would require an effort beyond the scope of this work. Typically the effect of heat exchanger fouling, primary system resistance uncertainty, pump uncertainties and control system errors (power and flowrate) on primary system inlet temperature are modeled using a Monte Carlo technique to ultimately yield hot spot factors for reactor inlet temperature and subchannel temperature rise (Ref. 2).

Even though such an analysis cannot be done here, we can and should make use of the work done for CRBR. Care must be exercised in borrowing numbers directly as the small LMR and CRBR are different plants: thus there is no guarantee that numbers are transferable. For CRBR a three sigma subfactor of 1.14 was applied to subchannel temperature rise. Without attempting to justify whether this number is valid here, it will be used in the absence of other values.

6.2.7 Loop Temperature Imbalance

This subfactor is unity since the primary system in the small LMR consists of a single loop.

6.2.8 Interassembly Flow Distribution

Although the fuel assembly flow distribution hardware can be plant specific, it will probably be similar to CRBR, thus the CRBR geometry will be assumed. For CRBR it was estimated that the test data upon which the hydraulic loss correlations for the inlet and outlet nozzles were based contributed a three sigma error of 0.018 to the calculated assembly flowrate while the orificing test data contributed 0.45. Manufacturing tolerances in flow distribution hardware, excluding the rod bundle which is characterized under Subchannel Flow Area, contributed a three sigma uncertainty of 0.013. A systematic error of 0.002 for assembly flowrate was estimated. These combine statistically to give a three sigma uncertainty of 0.05 in subchannel coolant temperature rise. Finally a direct bias error of 0.02 was assigned to cover any additional uncertainties.

6.2.9 Intraassembly Flow Distribution

As noted in Section 5, the errors in a subchannel calculation are dependent in part on the similarity between the geometry and the conditions being simulated and the geometry and the conditions for which the code was calibrated. As far as characterizing the errors in the temperatures predicted by SUPERENERGY-2 (Ref. 6) for the LMR assembly, it is appropriate at this point to estimate errors based on existing work. For this, we turn to the work done for CRBR.

It turns out that the CRBR and small LMR fuel assemblies both have 217 pins and that for the peak assemblies the power and flow differ by less than 30%. Hence the assemblies and their operating conditions are similar. Without pursuing how the parameter values for the CRBR subchannel code, COTEC, and our subchannel code, SUPERENERGY-2, were chosen; we will assume that the errors estimated for the CRBR subchannel code in Ref. 2 apply here. This may be conservative since the errors are proportional to the power skew across the bundle. CRBR errors are based on a power skew that is very large compared to the almost flat small LMR power skew.

The errors taken from CRBR (Ref. 2) are for the coolant, a direct uncertainty of 0.03 and a three sigma uncertainty of 0.058. The corresponding film temperature rise values are 0.006 and 0.005, respectively.

6.2.10 Subchannel Flow Area

A full fledged treatment of subchannel flow area uncertainty requires analysis of assembly manufacturing tolerances and of rod bowing with life. Although such an analysis is beyond the scope of this work, it is possible to borrow from the CRBR work to arrive at a very good estimate for the small LMR hot spot value.

To compute the hot spot subfactor, we begin with the assumption that the uncertainty in subchannel flow area is the same as for CRBR. This is the case with manufacturing errors, as wire wrap and pin diameter tolerances should be independent of the particular assembly dimensions. The assumption is probably conservative with respect to bowing since the degree of bowing is dependent on the assembly power skew and CRBR has the larger skew because of its heterogeneity.

Then following the method described in Appendix D, three standard deviations in CRBR area is, from Eq. D.3, 1.91E-7* m^2 based on a three sigma hot spot subfactor value of 1.019 and nominal channel area of 1.7E-5 m^2. The three sigma subfactor for the small LMR then is, from Eq. D.3, 1.010 where the small LMR subchannel area of 3.76E-5 m^2 and three standard deviations in area of 1.91e-7 have been used.

6.2.11 Wire Wrap Orientation

An analysis performed for CRBR fuel assemblies showed that the flow and temperature distribution in a subchannel depends slightly on the relative orientation of the wire wraps and the assembly power skew. This effect caused a less than 1% variation in temperature rise in the peak subchannel (Ref. 2). This effect should be much smaller in the small LMR since assembly power skews are much smaller than those found in CRBR. In CRBR large power gradients exist near blanket-fuel interfaces while here there are no blanket or control assemblies. The wire wrap subfactor, is therefore, set to unity.

6.2.12 Coolant Properties

The accuracy of the calculated film and subchannel temperature rises are dependent in part on the accuracy of coolant property correlations. For the subchannel with the peak nominal clad temperature, the subchannel coolant temperature rise is roughly 40 times that of the film temperature rise. Hence it is reasonable to look only at the uncertainties associated with the property correlations used in the subchannel temperature rise calculation. This calculation in SUPERENERGY-2 makes use of density and enthalpy properties only.

The NaK enthalpy correlation presently in SUPERENERGY-2 was taken from Ref. 8. There it is assigned a probable error of ±0.2%, which is interpreted arbitrarily here to mean that 50% of the time the measured value will fall within these bounds. If the measured values are assumed to have a normal distribution then this error is equivalently 0.6 standard derivations. Hence the three standard deviation uncertainty is 3.0*0.2/0.6 = 1%.

The NaK density correlation in SUPERENERGY-2 was taken from Ref. 9 which sites Ref. 10 as the origin. Reference 10 in turn sites Ref. 11 where finally the correlation is said to have come from Ref. 12. There the correlation is said to have an uncertainty of ±0.8%, but the nature of the uncertainty is not specifically stated. Due to various portions of text in the chain of references, the uncertainty is arbitrarily assumed to be equal to a three sigma uncertainty.

Combining the enthalpy and density uncertainties in quadrature gives a three sigma subchannel temperature rise uncertainty of 1.3%.

6.2.13 Film Heat Transfer Coefficient

The value of the subfactor is obviously dependent on the correlation used. The film temperature drop is calculated by hand using a correlation given in Ref. 4 with nominal temperatures and heat fluxes used in this calculation taken from SUPERENERGY-II and REBUS as described in Ref. 4. This correlation was also used for CRBR analysis of fuel assemblies and was chosen

*read as 1.91 × 10-7

there because it gave the most conservative results of a number of correlations looked at in Ref. 13.

As for the accuracy of this film heat transfer correlation, it was not obtained from experimental data based on prototypic small LMR fuel assembly dimensions and flow conditions. However, for the peak CRBR fuel assembly, the power and flow are within 30% of the small LMR values and the P/D ratios are close (1.24 for CRBR vs. 1.194). Thus the error in the correlation used here (i.e. in Ref. 4) should be approximately that which was used in CRBR. A three sigma subfactor of 1.12 was recommended for CRBR in Ref. 2. The same value will be used here.

6.2.14 Pellet Cladding Eccentricity

Since we will assume stacked mixed oxide pellets clad in stainless steel as does CRBR, the CRBR eccentricity subfactor is applicable. There may be some differences that result from different gap and pellet dimensions but these effects should be second order. They are even less important if one considers that the gap closes in the first few months after which time the subfactor is unity.

Another reason for adopting the CRBR results is that the analysis performed there is more detailed than could be pursued here. In the CRBR analysis the pellet was assumed to contact the cladding at a random circumferential location and the heat flux at this point was then calculated. Then for a concentric pellet the effect of the wire wrap on cladding temperature at the location where it made contact was calculated. These results were then combined to give the cladding midwall temperature for each direction of displacement. The result was a distribution of maximum cladding midwall temperature. From this came a direct subfactor of 1.14 and a three sigma subfactor of 1.174, both to be applied to film and cladding temperature drops.

6.2.15 Cladding Circumferential Temperature Distribution

As before, the level of detail carried out for CRBR goes beyond what can be done here with the computer codes available to us at present. Because of the similarity in fuel assembly geometry it is not unreasonable to use CRBR results until a similar analysis can be performed. For CRBR it was determined that to obtain peak circumferential midwall temperature, a direct hot spot factor of 1.6 to 1.9 should be applied to the nominal film temperature drop and 0.8 to the nominal cladding temperature drop.

6.2.16 Cladding Conductivity

As yet not much attention has been given to the choice of a conductivity correlation for the cladding material D-9. However, it is likely that the correlation used will be for unirradiated material and will have an uncertainty of about 5%, the same uncertainty as the correlations for stainless steels in Ref. 9. For the effect of irradiation on conductivity, Ref. 2 sites a study in which irradiation of cladding material is said to cause a change in conductivity of only a few percent. Until this is looked at in more detail, we will assume that the 5% uncertainty discussed above brackets the irradiation effects.

An uncertainty in cladding thickness also effects the cladding conductance. A thickness below the nominal reduces the local cladding midwall

temperature and therefore is not of interest as far as predicting the two sigma temperature. This is important as far as fuel pin failure analysis is concerned, however, since fuel pin lifetime is directly related to cladding thickness. For a thickness above the nominal it turns out that the net affect of the increased temperature rise and the increased structural robustness is an increase in fuel pin lifetime. Thus it is not necessary to include the affect of cladding thickness uncertainty in calculation of peak cladding temperatures.

A direct subfactor of 1.05 based on the 5% conductivity error for unirradiated material discussed above will be used.

6.2.17 Hot Channel Factors

If the vertical approach to the semistatistical method were used, hot channel factors would have been computed via Eq. A.25. However, since the horizontal approach is used, hot channel factor values are not computed or used.

6.2.18 Hot Channel Temperatures via Horizontal Method

The hot spot subfactors presented above are summarized in Table II. Using these values and the nominal temperatures at the peak cladding temperature location taken from Ref. 4, a two sigma cladding midwall temperature of 1268°F is calculated in Table III according to Eq. A.16.

6.2.19 Comparison With Previous 5 Factor Vertical Method

In this subsection, several numerical examples based on the small LMR are used to quantify the difference between the two sigma value as calculated consistent with past Applied Physics work and the value as calculated in accord with the semistatistical horizontal method recommended in this report.

There are three basic discrepancies between past and present approaches. First, past work made use of the vertical implementation of the semistatistical method instead of the horizontal implementation recommended here. Second, in the past, hot channel factors from CRBR were applied outright to other reactors without examining the validity of this transfer. Third, some of these hot channel factors were applied incorrectly.

To isolate the effect of each of these differences, a numerical example is worked through three times, each time with only one of the three discrepancies present. In each case, the hot spot temperature is first calculated as it would have been prior to this memo and then with the source of the discrepancy removed as this memo recommends. Finally an example is worked through with all discrepancies acting simultaneously. The details of the calculations are given in Appendix C so here we will discuss only the results. The results are summarized below and indicate that each discrepancy acting on its own causes a large temperature error relative to the recommended method. However when all three discrepancies act simultaneously, there is some cancellation of error and the net result is that the past method underestimates the cladding hot spot temperature only by 16 °F. Assuming the recommended method gives the correct answer, the error in the past method is not on the conservative side and hence the use of this method might result in cladding failure rates that exceed design specifications.

TABLE II. Small LMR Fuel Assembly Cladding Hot Spot Subfactors

	Coolant	Film	Cladding
Direct			
Measurement	1.0	1.0	1.0
Reactor physics models	1.06	1.06	1.06
Control rod banking	1.02	1.02	1.02
Interassembly flow distribution	1.02		
Intraassembly flow distribution	1.03	1.006	
Pellet cladding eccentricity		1.14	1.14
Cladding circumferential temperatures distribution		1.8	0.8
Cladding conductivity and thickness			1.05
Statistical (3σ)			
Fissile fuel distribution	1.052	1.052	1.052
Nuclear data	1.02	1.02	1.02
Balance of plant	1.14		
Loop temperature imbalance	1.0		
Interassembly flow distribution	1.05		
Intraassembly flow distribution	1.058	1.005	
Subchannel flow area	1.01		
Wire wrap orientation	1.0		
Coolant properties	1.013		
Film heat transfer coefficient		1.12	
Pellet cladding eccentricity		1.174	1.174

TABLE III. Calculation of Two Sigma Peak Cladding Midwall Temperature Using Horizontal Method and Small LMR Nominal Temperatures and CRBR Subfactors

	Inlet T	Coolant ΔT	Film ΔT	Cladding MW ΔT	Total
1. Nominal Temperatures (°F)	850	309	7	6	1172
2. 0σ Temperatures (°F)	850	351.0 (= 309·1.06·1.02·1.02·1.03)	15.6 (= 7.0·1.06·1.02·1.006·1.14·1.8)	6.2 (= 1.06·1.02·1.14·0.8·1.05·6.0)	
3. 3σ Temperature Uncertainties (°F)					
Fissile fuel distribution		18.3 (= 351.0·0.052)	0.8 (= 15.6·0.052)	0.3 (= 6.2·0.052)	19.4
Nuclear data		7.0	0.3	0.1	7.4
Balance of plant		49.1			49.1
Loop temperature imbalance		0			0
Interassembly flow distribution		17.6			17.6
Intraassembly flow distribution		20.4	0.1		20.5
Subchannel flow area		3.5			3.5
Wire wrap		0			0
Coolant properties		4.6			4.6
Film heat transfer coefficient			1.9		1.9
Pellet cladding eccentricity			2.7	1.1	3.8
					$[\Sigma(3\sigma_i)^2]^{1/2} = 60.2$

4. 2σ Peak Cladding Midwall Temperature (°F)

$$T_{clad}^{2\sigma} = 850 + (351.0 + 15.6 + 6.2) + \frac{2}{3}(60.2) = 1263$$

Comparison of Recommended Method with Past

Point of Comparison	Past	Recommended
1. Degree of conservatism (Section C.1)	1266 (°F) (Semistatistical vertical method, Table C.1)	1263 (Semistatistical horizontal method, Table III)
2. Validity of uncertainty data (Section C.2)	1282 (Outside validity range, Table C.3)	1263 (Within validity range, Table III)
3. Correctness of application of uncertainty data (Section C.3)	1247 (Omissions, errors, Table C.4)	1275 (Correct, Table C.5)
4. All of the above (Section C.4)	1247 (Table C.4)	1263 (Table III)

One final note regarding the use of data for characterizing uncertainties. The numerical results of Section C.2 substantiate what was recognized by Malloy while writing Ref. 4, that the origin and limitations of uncertainty data used in the Division in the past has become obscured with time and that these data may have been useful for an expedient calculation but that its legitimacy should have been viewed with caution. It appears that such reservations were justified and that the development of subfactor data and the method of applying it as described in this work is preferred to the 5 factor vertical method which has been used in the past.

6.3 Fuel Hot Spot

The calculation of fuel centerline hot spot temperature is identical to that performed to get the cladding hot spot temperature, except that a different set of hot spot values is used and that subfactors for gap and fuel are required. Subfactors which are new from the cladding case or whose values change are given below.

The location of the fuel centerline hot spot was found in Ref. 4 to be at the core midplane. The procedure used to find it is identical to that described for the cladding hot spot in Section 6.2.

6.3.1 Pellet Cladding Eccentricity

Although the effect of nonconcentric pellet alignment is to elevate cladding temperature at the point of minimum gap, this is a localized effect. The fuel centerline temperature is actually lowered below nominal because of overall enhanced heat transfer. Therefore for fuel temperature calculations, the pellet-cladding eccentricity subfactor can be set to unity.

6.3.2 Cladding Circumferential Temperature Distribution

The relatively large conductance path between pellet surface and ceterline averages out local hot spots on the pellet surface from the fuel centerline temperature. The net effect on the centerline temperature is the same as if the coolant had a uniform mixed mean temperature. Since the subchannel codes work with coolant averages, the fuel centerline temperature computed should be the same as the actual case where the coolant has a circumferential distribution. Hence a subfactor of unity is assigned.

6.3.3 Pellet Cladding Gap Conductance

The gap conductance is a complicated function of gap thickness, gas pressure, gas composition and fuel/cladding contact. In addition each of these factors is itself the result of complex processes. Therefore we do not attempt to decompose there errors here but instead will use results from CRBR which had a pin geometry identical to the small LMR design. From Ref. 3, the three sigma uncertainty in clad conductance at the location of peak fuel centerline temperature is 0.48.

6.3.4 Fuel Conductivity

The fuel conductivity is dependent on fuel density and plutonium content, both of which vary with pellet fabrication batch. In addition burnup changes the conductivity. For CRBR in Ref. 3, these effects were estimated to cause a maximum reduction in conductivity of 10%.

6.3.5 Hot Channel Temperature via Horizontal Method

The subfactors for the fuel centerline temperature are represented in Table IV and consist of the cladding subfactors after having made the changes described above. Using these values and the nominal temperatures at the peak fuel centerline temperature location taken from Ref. 4, a two sigma fuel centerline temperature of 2523°F is calculated in Table V according to Eq. A.16.

6.3.6 Comparison With the 5-Factor Vertical Method

The calculation of two sigma fuel centerline temperature by means of the 5-factor vertical method is subject to the same criticisms as were made in Appendix C for the cladding temperature calculation. They are therefore not repeated here. The value gotten via the old method is from Ref. 4, revision of June 14, 1984, 2649 (°F) which compares with 2523 (°F) computed in Table V using the horizontal method recommended in this work.

TABLE IV. Small LMR Fuel Assembly Fuel Centerline Hot Spot Subfactors

	Coolant	Film	Cladding	Gap	Fuel
Direct					
Measurement	1.0	1.0	1.0	1.0	1.0
Reactor physics models	1.06	1.06	1.06	1.06	1.06
Control rod banking	1.02	1.02	1.02	1.02	1.02
Interassembly flow distribution	1.02				
Intraassembly flow distribution	1.03	1.006			
Pellet cladding eccentricity		1.0	1.0		
Cladding circumferential temperature distribution		1.0	1.0		
Cladding conductivity and thickness			1.05		
Statistical (3σ)					
Fissile fuel distribution	1.052	1.052	1.052	1.052	1.052
Nuclear data	1.02	1.02	1.02	1.02	1.02
Balance of plant	1.14				
Loop temperature imbalance	1.0				
Interassembly flow distribution	1.05				
Intraassembly flow	1.058	1.005			
Subchannel flow area	1.01				
Wire wrap orientation	1.0				
Coolant properties	1.013				
Film heat transfer coefficient		1.12			
Pellet cladding eccentricity		1.0	1.0		
Gap conductance				1.48	
Fuel conductivity					1.1

TABLE V. Calculation of Two Sigma Fuel Centerline Temperature at Core Midplane Using Horizontal Method and Small LMR Nominal Temperatures and CRBR Subfactors

	Inlet T	Coolant ΔT	Film ΔT	Cladding ΔT	Gap ΔT	Fuel ΔT	Total
1. Nominal Temperatures (°F)	850	160	25	43	265	928	2271
2. Oσ Temperatures (°F)	850	181.7	27.2	48.8	286.5	1003	
3. 3σ Temperature Uncertainties (°F)							
Fissile fuel distribution		9.4	1.4	2.5	14.9	52.2	80.4
Nuclear data		3.6	0.5	1.0	5.7	20.1	30.9
Balance of plant		25.4					25.4
Loop temperature imbalance		0					0
Interassembly flow distribution		9.1					9.1
Intraasembly flow distribution		10.5	0.1				10.6
Subchannel flow area		1.8					1.8
Wire wrap		0					0
Coolant properties		2.4					2.4
Film heat transfer coefficient			3.3				3.3
Pellet cladding eccentricity			0	0			0
Gap conductance					137.5		137.5
Fuel conductivity						92.8	92.8
						$[\Sigma(3\sigma_1)^2]^{1/2}$ =	189.2

4. 2σ Peak Fuel Centerline Temperature (°F)

$$T_{fuel}^{2\sigma} = 850 + (181.7 + 27.2 + 48.8 + 286.5 + 1003) + \frac{2}{3}(189.2) = 2523$$

7. SUMMARY, RECOMMENDATIONS AND CONCLUSIONS

Hot spot analyses are a standard part of core thermal hydraulic design. The principle requirement of any hot spot method is that it be defensible. A candidate method must have a rigorous analytic basis, permit treatment of different error types, have been shown to give realistic temperature estimates and use input data that can be obtained based on measurements or estimates.

A review of the hot spot methods used in the Applied Physics Division was made as part of an upgrading of core thermal hydraulic capabilities. It was found that very little documentation exists and hence it is difficult to determine whether the hot spot methods used in the Division meet the criteria above. For this reason the methods that have been used in the past are difficult to defend. It also appears that a formal assessment of the Division's requirements has never been made.

A fresh look at hot spot analysis methods was undertaken. The Division requires a method that meets the four criteria described above and additionally is amenable to computer solution so it can be used in routine design applications. A review of the principle hot spot methods was made and it was determined that the semistatistical horizontal method best meets our needs. Perhaps the strongest point in favor of using this method is that it was applied to CRBR and received extensive scrutiny there. The semistatistical horizontal method is now available as an option in SE2-ANL. It is also recommended that more attention in the future be given to finding appropriate subfactor values for uncertainties that are reactor specific.

8. REFERENCES

1. Carelli, M. D. and Friedland, A. J., "Hot Channel Factors for Rod Temperature Calculations in LMFBR Assemblies," Nuclear Engineering and Design 62, 1980.

2. Friedland, A. J., "CRBRP Core Assemblies Hot Channel Factors Preliminary Analysis," CRBRP-ARD-0050, February 1980.

3. Carelli, M. D. and Spencer, D. R., "CRBRP Assemblies Hot Channel Factors Preliminary Analysis," WARD-D-0050, October 1974.

4. Malloy, D. J. and Chang, Y. I., "Temperature Data for the 6.5 Foot DTR Core," Argonne National Laboratory, Intra-Laboratory Memorandum, April 11, 1984.

5. LeSage, L. G., et al., "International Comparison Calculation of a Large Sodium-Cooled Fast Breeder Reactor," Proceedings, ANL-80-78, August 1980.

6. Basehore, K. L. and Todreas, N. E., SUPERENERGY-2: A Multiassembly, Steady-State Computer Code for LMFBR Core Thermal-Hydraulic Analysis," PNL-3379, August 1980.

7. El-Wakil, M. M., "Nuclear Heat Transport," American Nuclear Society, 1978.

8. Douglas, T. B., Ball, F. B., and Ginnings, D. C., Heat Capacity of Potassium-Sodium Alloys Between 0 and 800 degrees C," AECU-1017.

9. Nuclear Systems Materials Handbook, TID 26666, Hanford Engineering Development Laboratory, Richland, Washington.

10. Liquid Metal Information Center, P.O. Box 1449, Canoga Park, CA 91304.

11. Foust, O. J., "Sodium-NaK Engineering Handbook," Vol. 1, Gordan and Breach, Science Publishers, 1976.

12. Ewing, C. T., Atkinson, Jr., H. B., and Rice, T. K., Quarterly Progress Report No. 7 on the Measurements of the Physical and Chemical Properties of the Sodium-Potassium Alloy, USAEC File No. NP-340, Naval Research Laboratory, May 24, 1948.

13. Meyer, P. L., "Introductory Probability and Statistics," Addison-Wesley, 1972.

APPENDIX A: SEMISTATISTICAL METHOD

This appendix derives the semistatistical method from first principles. It is shown that by introducing the appropriate mathematical inequalities, the horizontal, vertical and vertical heat flux forms are derivable from the sum of square form. It is also shown that the sum of squares form gives the smallest two sigma temperature value followed in order by the horizontal, vertical and vertical heat flux forms.

A.1 Dependence of Temperature on Uncertainties

The semistatistical method provides a means of representing the effect of analytic and manufacturing uncertainties on fuel pin temperature at a given location. The method assumes that the temperature is affected by the uncertainties as follows

$$T_M(\underline{\alpha},\underline{\varepsilon}) = T_o + \varepsilon_1 + \sum_{i=1}^{M} \Delta T_i\ (\underline{\alpha},\underline{\varepsilon}) \qquad (A.1)$$

where

$\underline{\alpha}$ = vector of deterministic errors of dimension k,

$\underline{\varepsilon}$ = vector of random errors of dimension n having mean $\underline{0}$ and standard deviation $\underline{\sigma}$,

T_o = nominal subchannel inlet temperature,

$\Delta T_i\ (\underline{\alpha},\underline{\varepsilon})$ = ith temperature rise,

$T_M\ (\underline{\alpha},\underline{\varepsilon})$ = temperature at location M.

As an illustration consider cladding midwall temperature. The temperature is the sum of the reactor inlet temperature T_o, a random error ε_1, the subchannel coolant temperature rise ΔT_1, the film temperature rise ΔT_2 and the cladding midwall temperature rise ΔT_3. Each of the temperature rises is a function of random errors $\underline{\varepsilon}$ and bias errors $\underline{\alpha}$.

The statistical properties of Eq. (A.1) cannot be evaluated without first introducing several approximations. From the definition of the total differential

$$\Delta T_i\ (\underline{\alpha},\underline{\varepsilon}) - \Delta T_i\ (\underline{\alpha},\underline{0}) \tilde{=} \sum_{j=1}^{n} \Delta T_i\ (\underline{\alpha},0\ldots\varepsilon_j\ldots 0) - \Delta T_i\ (\underline{\alpha},0) \qquad (A.2)$$

so that Eq. A.1 becomes

$$T_M\ (\underline{\alpha},\underline{\varepsilon}) = T_o + \varepsilon_1 + \sum_{i=1}^{M} \Delta T_i\ (\underline{\alpha},\underline{0}) + \sum_{j=1}^{n} \Delta T_i\ (\underline{\alpha},\ldots\varepsilon_j\ldots 0) - \Delta T_i\ (\underline{\alpha},\underline{0}) \qquad (A.3)$$

The direct subfactor is defined as

$$f_{i\ell}^{D} = \frac{\Delta T_i(0\ldots\alpha_\ell\ldots0,\underline{Q})}{\Delta T_i(\underline{Q},\underline{Q})} .$$

and the statistical subfactor is

$$f_{ij}^{S}(\varepsilon_j) = \frac{\Delta T_i(\underline{Q},0\ldots\varepsilon_j\ldots0)}{\Delta T_i(\underline{Q},\underline{Q})}$$

From the definition of the direct subfactor

$$\Delta T_i\ (\alpha_1,\alpha_2,\ldots0,\underline{Q}) = f_{i1}^{D}\ (\alpha_1)\ \Delta T_i\ (0,\alpha_2\ldots0,\underline{Q}) = f_{i1}^{D}\ (\alpha_1)\ f_{i2}^{D}\ (\alpha_2)\ \Delta T_i\ (\underline{Q},\underline{Q})$$

so that sucessive applications give

$$\Delta T_i\ (\underline{\alpha},\underline{Q}) = \Delta T_i\ (\underline{Q},\underline{Q}) \prod_{\ell=1}^{k} f_{i\ell}^{D}\ (\alpha_\ell) \qquad (A.4)$$

From the definition of the statistical subfactor, the approximation

$$\frac{\Delta T_i(\underline{\alpha},0\ldots\varepsilon_j\ldots0)}{\Delta T_i(\underline{\alpha},\underline{Q})} = \frac{\Delta T_i(\underline{Q},0\ldots\varepsilon_j\ldots0)}{\Delta T_i(\underline{Q},\underline{Q})}$$

and Eq. (A.4)

$$\Delta T_i(\underline{\alpha},0\ldots\varepsilon_j\ldots0) = f_{ij}^{S}\ (\varepsilon_j)\ \Delta T_i\ (\underline{Q},0) \prod_{\ell=1}^{k} f_{i\ell}^{D} \qquad (A.5)$$

The temperature at the hot spot, expressed in terms of nominal temperature rises and uncertainty subfactors, is upon substitution of Eq. (A.4) and (A.5) into Eq. (A.3)

$$T_M\ (\underline{\alpha},\underline{\varepsilon}) = T_o + \varepsilon_1 + \sum_{i=1}^{M} \Delta T_i\ (\underline{Q},\underline{Q}) \prod_{\ell=1}^{k} f_{i\ell}^{D}\ (\alpha_\ell) \qquad (A.6)$$

$$\sum_{j=1}^{n} \left(f_{ij}^{S}(\varepsilon_j) - 1\right) \Delta T_i\ (\underline{Q},\underline{Q}) \prod_{\ell=1}^{k} f_{i\ell}^{D}\ (\alpha_\ell)$$

A.2 Mean and Variance

Obtaining an expression for the two sigma temperature requires evaluating the mean and variance of $T_M(\underline{\alpha},\underline{\varepsilon})$ as given by Eq. (A.6). To evaluate these we make use of the following results from the theory of random variables (Ref. 13).

Result 1: Let $\chi_1, \chi_2, \ldots \chi_n$ be a sequence of independent random variables with mean μ_i and variance σ_i^2, i=1, 2 ... n. Let $\chi = \chi_1 + \chi_2 + \ldots + \chi_n$. Then

$$Z_n = \frac{\chi - \sum_{i=1}^{n} \mu_i}{\sum_{i=1}^{n} \sigma_i^2}$$

has approximately a normal distribution with mean 0 and variance 1. Alternatively, the mean of χ is the sum of individual χ_i means and the variance of χ is the sum of individual χ_i variances.

Result 2: If χ is a random variable with mean μ and variance σ^2 and if y is a function of χ defined through $y=h(\chi)$ then

$$\text{mean of } y \tilde{=} h(\mu) + \frac{h''(\mu)}{2} \sigma^2 \qquad \text{(A.7a)}$$

$$\text{variance of } y \tilde{=} [h'(\mu)]^2 \sigma^2 \qquad \text{(A.7b)}$$

where the prime sign designates differentiation.

For the mean of $T_M(\underline{\alpha},\underline{\varepsilon})$, note that apart from the ε_1 term, only the summation over j in Eq. (A.6) is a random variable, or more specifically, $f_{ij}^S(\varepsilon_j)$. From Result 2, the mean of this quantity is gotten by substituting into it and its second derivative, $\varepsilon_j = 0$. But the second derivative should be very small since $f_{ij}^S(\varepsilon_j)$ is typically a smooth varying function of ε_j. Since $f_{ij}^S(\varepsilon_j)$ is unity the mean of $T_M(\underline{\alpha},\underline{\varepsilon})$ is therefore

$$\text{mean}\left[T_M(\underline{\alpha},\underline{\varepsilon})\right] = T_o + \sum_{i=1}^{M} \Delta T_i(\underline{0},\underline{0}) \prod_{\ell=1}^{k} f_{i\ell}^D \qquad \text{(A.8)}$$

where

$$f_{i\ell}^D = f_{i\ell}^D(\alpha_\ell) .$$

For the variance of $T_M(\underline{x},\underline{\xi})$, we assume that the random variables f^s_{ij} in Eq. (A.6) are uncorrelated over all i and j. Then the variance of Eq. (A.6) is from Result 1, the sum of the variance of each individual term. Noting that the variance of ϵ_j is σ_j^2, making use of Eq. (A.7b) and approximating the derivative in Eq. (A.7b) with first order differencing gives

$$\text{variance}\left[f^s_{ij}(\epsilon_j) - 1\right] = (f^s_{ij|\sigma} - 1)^2$$

where

$$f^s_{ij|\sigma}{}^2 = \text{variance}\left[f^s_{ij}(\epsilon_j)\right] .$$

Then

$$\text{variance}\left[T_M(\underline{x},\underline{\xi})\right] = \sigma_1^2 + \sum_{i=1}^{M}\sum_{j=1}^{n}(f^s_{ij|\sigma} - 1)^2 \left(\Delta T_i(\underline{0},\underline{0}) \prod_{\ell=1}^{k} f^D_{i\ell}\right)^2 \quad (A.9)$$

A.3 Sum of Squares Form

The sum of squares expression for the two sigma temperature estimate can be used to derive the three other forms. The expression is obtained directly from the two sigma definition,

$$T_M^{2\sigma}(\underline{x},\underline{\xi}) = \text{mean}\left[T_M(\underline{x},\underline{\xi})\right] + 2\left[\text{variance}\left[T_M(\underline{x},\underline{\xi})\right]\right]^{1/2} \quad (A.10)$$

Substituting Eq. (A.8) and (A.9) into Eq. (A.10) gives the sum of squares form

$$T^{2\sigma}_{Mss}(\underline{x},\underline{\xi}) = T_o + \sum_{i=1}^{M}\Delta T_i(\underline{0},\underline{0}) \prod_{\ell=1}^{k} f^D_{i\ell} \quad (A.11)$$

$$+ 2\left[\sigma_1^2 + \sum_{i=1}^{M}\sum_{j=1}^{n}(f^s_{ij|\sigma} - 1)^2 \left(\Delta T_i(\underline{0},\underline{0}) \prod_{\ell=1}^{k} f^D_{i\ell}\right)^2\right]^{1/2}$$

The derivation of the remaining three other forms of the two sigma estimate is given in the rest of the appendix. The following definitions are used,

$$a = T_o + \sum_{i=1}^{M}\Delta T_i(\underline{0},\underline{0}) \prod_{\ell=1}^{k} f^D_{i\ell}$$

$$b^2 = \sigma_1^2 \quad (A.12)$$

$$c_{ij}^2 = (f^s_{ij1\sigma} - 1)^2$$

$$d_i^2 = (\Delta T_i(\underline{Q},\underline{Q}) \prod_{\ell=1}^{k} f^D_{i\ell})^2 .$$

With these definitions, Eq. (A.11) becomes,

$$T^{2\sigma}_{M_{ss}}(\underline{a},\underline{\xi}) = a + 2\left\{b^2 + \sum_{i=1}^{M}\sum_{j=1}^{n} c_{ij}^2 d_i^2\right\}^{1/2} \tag{A.13}$$

A.4 Horizontal Form

Define

$$T^{2\sigma}_{M_H}(\underline{a},\underline{\xi}) = a + 2\left\{b^2 + \sum_{j=1}^{n}\left(\sum_{i=1}^{M} c_{ij}d_i\right)^2\right\}^{1/2} \tag{A.14}$$

Then from the inequality

$$\sum_{i=1}^{M}\sum_{j=1}^{N} c_{ij}^2 d_i^2 \le \sum_{j=1}^{n}\left(\sum_{i=1}^{M} c_{ij}d_i\right)^2$$

and Eq. (A.13) we obtain the result

$$T^{2\sigma}_{M_H}(\underline{a},\underline{\xi}) \ge T^{2\sigma}_{M_{SS}}(\underline{a},\underline{\xi}) . \tag{A.15}$$

Substituting the definitions of Eq. (A.12) into Eq. (A.14), the horizontal form is

$$T^{2\sigma}_{M_H}(\underline{a},\underline{\xi}) = T_o + \sum_{i=1}^{M} \Delta T_i(\underline{Q},\underline{Q}) \prod_{\ell=1}^{k} f^D_{i\ell}$$

$$+ 2\left\{\sigma_1^2 + \sum_{j=1}^{n}\left[\sum_{i=1}^{M}(f^s_{ij1\sigma} - 1)\,\Delta T_i(\underline{Q},\underline{Q}) \prod_{\ell=1}^{k} f^D_{i\ell}\right]^2\right\}^{1/2} \tag{A.16}$$

From Eq. (A.15), the two sigma estimate obtained from the horizontal form is equal to or greater than that obtained from the sum of squares form.

A.5 Vertical Form

The vertical form is obtained from the horizontal form as follows. In Eq. (A.15), the summation over j is rearranged so that

$$\sum_{j=1}^{n} \left(\sum_{i=1}^{M} c_{ij} d_i \right)^2 = \sum_{j=1}^{n} \left[\sum_{i=1}^{M} (c_{ij} d_i)^2 + 2 \sum_{k=1}^{M} \sum_{\ell=k+1}^{M} c_{kj} d_k \, c_{\ell j} d_\ell \right]$$

$$= \sum_{i=1}^{M} d_i^2 \sum_{j=1}^{n} c_{ij}^2 + 2 \sum_{k=1}^{M} \sum_{\ell=k+1}^{M} d_k d_\ell \sum_{j=1}^{n} c_{kj} c_{\ell j} \qquad \text{(A.17)}$$

An alternate expression for the first summation over i on the right hand side of Eq. (A.17) is sought. To obtain it, note that

$$\left[\sum_{i=1}^{M} d_i \left(\sum_{j=1}^{n} c_{ij}^2 \right)^{1/2} \right]^2 = \sum_{i=1}^{M} d_i^2 \sum_{j=1}^{n} c_{ij}^2 + 2 \sum_{k=1}^{M} \sum_{\ell=k+1}^{M} d_\ell d_k \left(\sum_{j=1}^{n} c_{kj}^2 \right)^{1/2} \left(\sum_{j=1}^{n} c_{\ell j}^2 \right)^{1/2}$$

which when rearranged is

$$\sum_{i=1}^{M} d_i^2 \sum_{j=1}^{n} c_{ij}^2 = \left[\sum_{i=1}^{M} d_i \left(\sum_{i=1}^{n} c_{ij}^2 \right)^{1/2} \right]^2 - 2 \sum_{k=1}^{M} \sum_{\ell=k+1}^{M} d_\ell d_k \left(\sum_{j=1}^{n} c_{kj}^2 \right)^{1/2} \left(\sum_{j=1}^{n} c_{\ell j}^2 \right)^{1/2} \qquad \text{(A.18)}$$

Substituting Eq. (A.18) into Eq. (A.17) gives

$$\sum_{j=1}^{n} \left(\sum_{i=1}^{M} c_{ij} d_i \right)^2 = \left[\sum_{i=1}^{M} d_i \left(\sum_{j=1}^{n} c_{ij}^2 \right)^{1/2} \right]^2 - 2 \sum_{k=1}^{M} \sum_{\ell=k+1}^{M} d_\ell d_k \left(\sum_{j=1}^{n} c_{kj}^2 \right)^{1/2} \left(\sum_{j=1}^{n} c_{\ell j}^2 \right)^{1/2}$$

$$+ 2 \sum_{k=1}^{M} \sum_{\ell=k+1}^{M} d_k d_\ell \sum_{j=1}^{n} c_{kj} c_{\ell j}$$

and collecting terms yields

$$\sum_{j=1}^{n} \left(\sum_{i=1}^{M} c_{ij} d_i \right)^2 = \left[\sum_{i=1}^{M} d_i \left(\sum_{j=1}^{n} c_{ij}^2 \right)^{1/2} \right]^2$$

$$+ 2 \sum_{k=1}^{M} \sum_{\ell=k+1}^{M} d_\ell d_k \left[\left(\sum_{j=1}^{n} c_{kj} c_{\ell j} \right) - \left(\sum_{j=1}^{n} c_{kj}^2 \right)^{1/2} \left(\sum_{j=1}^{n} c_{\ell j}^2 \right)^{1/2} \right] \qquad \text{(A.19)}$$

Equation (A.19) is the form sought for the left side of Eq. (A.17). Making use of the Cauchy Schwarz inequality

$$\left(\sum_{j=1}^{n} c_{kj} c_{\ell j} \right) - \left(\sum_{j=1}^{n} c_{kj}^2 \right)^{1/2} \left(\sum_{j=1}^{n} c_{\ell j}^2 \right)^{1/2} \leq 0$$

we obtain from Eq. (A.19)

$$\sum_{j=1}^{n} \left(\sum_{i=1}^{M} c_{ij} d_i \right)^2 \leq \left[\sum_{i=1}^{M} d_i \left(\sum_{j=1}^{n} c_{ij}^2 \right)^{1/2} \right]^2 \qquad \text{(A.20)}$$

Now from the triangle inequality and Eq. (A.20)

$$\left\{b^2 + \sum_{j=1}^{n} \left(\sum_{i=1}^{M} c_{ij} d_i \right)^2 \right\}^{1/2} \leq b + \left\{ \sum_{j=1}^{n} \left(\sum_{i=1}^{M} c_{ij} d_i \right)^2 \right\}^{1/2}$$

$$\leq b + \sum_{i=1}^{M} d_i \left(\sum_{j=1}^{n} c_{ij}^2 \right)^{1/2} \tag{A.21}$$

Define

$$T_{m_V}^{2\sigma} (\underline{\alpha}, \underline{\xi}) = a + 2 \left\{ b + \sum_{i=1}^{M} d_i \left(\sum_{j=1}^{n} c_{ij}^2 \right)^{1/2} \right\} \tag{A.22}$$

Then from the inequality of Eq. (A.21) and the definitions of Eq. (A.22) and (A.14), we obtain

$$T_{M_V}^{2\sigma} (\underline{\alpha}, \underline{\xi}) \geq T_{M_H}^{2\sigma} (\underline{\alpha}, \underline{\xi}) \tag{A.23}$$

Substituting the definitions of Eq. (A.12) into Eq. (A.22), the <u>vertical form</u> is

$$T_{M_V}^{26} (\underline{\alpha}, \underline{\xi}) = T_o + 2\sigma_1 + \sum_{i=1}^{M} \Delta T_i (\underline{0}, \underline{0}) \prod_{\ell=1}^{K} f_{i\ell}^D$$

$$+ 2 \sum_{i=1}^{M} \Delta T_i (\underline{0}, \underline{0}) \prod_{\ell=1}^{k} f_{i\ell}^D \left\{ \sum_{j=1}^{n} \left[(f_{ij1\sigma}^s - 1) \right]^2 \right\}^{1/2} \tag{A.24}$$

This can be written in a more compact form if we define

$$f_i = \prod_{\ell=1}^{k} f_{i\ell}^D \left\{ 1 + \left[\sum_{j=1}^{n} \left((f_{ij1\sigma}^s - 1) \right)^2 \right]^{1/2} \right\} \tag{A.25}$$

so that

$$T_{M_V}^{26} (\underline{\alpha}, \underline{\xi}) = T_o + 2\varepsilon_1 + \sum_{i=1}^{M} f_i \Delta T_i (\underline{0}, \underline{0}) \tag{A.26}$$

where f_i is the i^{th} <u>hot channel factor</u>.

From Eq. (A.23), the two sigma estimate obtained from the vertical form is equal to or greater than that obtained from the horizontal form.

A.6 Vertical Heat Flux Form

This form of the semistatistical method is a variation on the vertical form presented in the previous section. The variation has to do with the combining of local heat flux uncertainty subfactors. In the vertical form, the effect of uncertainty in local heat flux on film, cladding, gap or fuel temperature rise due to a single uncertainty (e.g. fissile maldistribution) is represented by a subfactor applied to the effected temperature rise). These subfactors are then collapsed into a single hot channel factor applied to the temperature rise as shown in Eq. (A.25). In the vertical heat flux form, however, the heat flux subfactors are combined into their own hot channel factor. This hot channel factor then premultiplies the usual hot channel factor to give a two sigma temperature according to

$$T^{2\sigma}_{M_{VHF}} = T_{in} + \varepsilon_i + \Delta T_{coolant} f_{coolant} + \Delta T_{film} f_{heat\ flux} f_{film} + \Delta T_{cladding} f_{heat\ flux} f_{cladding} \quad (A.27)$$

where

ΔT_i = ith temperature rise

f_i = hot channel factor associated with ΔT_i

$f_{heat\ flux}$ = hot channel factor for heat flux uncertainty

The vertical heat flux form estimate of the two sigma temperature is defined by

$$T^{2\sigma}_{M_{VHF}} = To + 2\varepsilon_1 + \sum_{i=1}^{M} f_{ih} f_{i\vec{h}} \Delta T_i (\underline{Q},\underline{Q}) \quad (A.28)$$

where

$$f_{ih} = \prod_{\ell=1}^{r} f^{D}_{ilh} \left\{1 + 2\left[\sum_{j=1}^{p} (f^{s}_{ijh} - 1)^2\right]\right\}$$

$$f_{i\vec{h}} = \prod_{\ell=1}^{k-r} f^{D}_{il\vec{h}} \left\{1 + 2\left[\sum_{j=1}^{n-p} (f_{ij\vec{h}} - 1)^2\right]\right\}$$

and

k = number of direct uncertainties

n = number of statistical uncertainties

r = number of direct uncertainties associated with local heat flux

p = number of statistical uncertainties associated with local heat flux

f^s_{ijh}, f^D_{ijh} = hot spot subfactors associated with heat flux uncertainties

$f^s_{ij\bar{h}}$, $f^D_{ij\bar{h}}$ = hot spot subfactors associated with non-heat flux uncertainties

To show that this expression yields a higher two sigma estimate than the vertical form, let

$$a = 4 \sum_{j=1}^{p} (f^s_{ijh} - 1)^2 \qquad b = 4 \sum_{j=1}^{n-p} (f_{ij\bar{h}} - 1)^2$$

so that

$$\begin{aligned} 1 + \sqrt{a+b} &\leq 1 + \sqrt{a+b} + \sqrt{ab} \\ &\leq 1 + \sqrt{a} + \sqrt{b} + \sqrt{ab} \\ &= (1 + \sqrt{a})\,(1 + \sqrt{b}) \end{aligned} \tag{A.29}$$

From the definition of fi in Eq. (A.25)

$$f_i = \prod_{\ell=1}^{r} f^D_{ilh} \prod_{\ell=1}^{k-r} f^D_{il\bar{h}} \left\{1 + 2\left[\sum_{j=1}^{p} (f^s_{ijh} - 1)^2 + \sum_{j=1}^{n-p} (f_{ij\bar{h}} - 1)^2\right]^{1/2}\right\} \tag{A.30}$$

Making use of the inequality given by Eq. (A.29), the following inequality holds

$$f_i \leq f_{ih}\, f_{i\bar{h}} \tag{A.31}$$

Substituting Eq. (A.31) into Eq. (A.28) and comparing with (A.26) yields

$$T^{2\sigma}_{M_{VHF}} \geq T^{2\sigma}_{M_V}$$

i.e. the two sigma estimate obtained from the vertical heat flux form is equal to or greater than that obtained from the vertical form.

APPENDIX B: SEMISTATISTICAL METHOD EXTENDED TO BALANCE OF PLANT UNCERTAINTIES

The semistatistical method is extended here to include treatment of those uncertainties outside the core that impact core temperature. The starting point is the recognition that these uncertainties affect the core only through reactor inlet temperature and reactor mass flowrate. In general the flowrate and inlet temperature uncertainty are correlated. Since the standard semistatistical treatment assumes independent uncertainties, they can not be handled by the method without modification. The standard semistatistical methodology of Appendix A is extended as follows. The general expression for temperature at point M is

$$T_M(\delta T_o, \delta W_R, \underline{\alpha}, \underline{\varepsilon}) = T_o + \delta T_o + \varepsilon_1 + \Delta T_c(\delta W_R, \underline{\alpha}, \underline{\varepsilon}) + \sum_{i=2}^{M} \Delta T_i(\underline{\alpha}, \underline{\varepsilon}) \quad (B.1)$$

where

δT_o = error in reactor inlet temperature due to uncertainty in the balance of plant

δW_R = error in reactor flowrate due to uncertainty in the balance of plant

ε_1 = error in subchannel inlet temperature due to inlet plenum modeling uncertainty

$\Delta T_c(\delta W_R, \underline{\alpha}, \underline{\varepsilon})$ = subchannel coolant temperature rise

and all other symbols are as defined in Appendix A.

As in Appendix A, the objective is to compute the mean and variance of Eq. (B.1) so that a two sigma temperature can be obtained. First we define

$$\delta\Delta T_c(\delta W_R) = \Delta T_c(\delta W_R, \underline{0}, \underline{0}) - \Delta T_c(0, \underline{0}, \underline{0}) \quad (B.2)$$

which is the error in subchannel temperature rise that results from a perturbation in the reactor flowrate. From the definition of the total differential

$$\Delta T_c(\delta W_R, \underline{\alpha}, \underline{\varepsilon}) - \Delta T_c(0, \underline{0}, \underline{0}) = \Delta T_c(\delta W_R, \underline{0}, \underline{0}) - \Delta T_c(0, \underline{0}, \underline{0}) + \left(\Delta T_c(0, \underline{\alpha}, \underline{\varepsilon}) - \Delta T_c(0, \underline{0}, \underline{0})\right) \quad (B.3)$$

so that from Eq. (B.2) and (B.3)

$$\Delta T_c(\delta W_R, \underline{\alpha}, \underline{\varepsilon}) = \delta\Delta T_c(\delta W_R) + \Delta T_c(o, \underline{\alpha}, \underline{\varepsilon}) \tag{B.4}$$

Substituting Eq. (B.4) into Eq. (B.1)

$$T_M(\delta T_o, \delta W_R, \underline{\alpha}, \underline{\varepsilon}) = T_o + \delta T_o + \varepsilon_1 + \delta\Delta T_c(\delta W_R) + \sum_{i=1}^{M} \Delta T_i(\underline{\alpha}, \underline{\varepsilon}) \tag{B.5}$$

Next assume that the subchannel and reactor coolant temperature rises are related by

$$\Delta T_c(\delta W_R, \underline{Q}, \underline{Q}) = c\, \Delta T_R(\delta W_R)$$

so that

$$\delta\Delta T_c(\delta W_R) = c\, \delta\Delta T_R(\delta W_R) \tag{B.6}$$

where

$\Delta T_R(\delta W_R)$ = reactor coolant temperature rise as a function of a flowrate perturbation from the nominal

and

$$\delta\Delta T_R(\delta W_R) = \Delta T_R(\delta W_R) - \Delta T_R(0).$$

Substituting Eq. (B.6) into Eq. (B.5)

$$T_M(\delta T_o, \delta W_R, \underline{\alpha}, \underline{\varepsilon}) = T_o + \delta T_o + \varepsilon_1 + c\, \delta\Delta T_R(\delta W_R) + \sum_{i=1}^{M} \Delta T_i(\underline{\alpha}, \underline{\varepsilon}) \tag{B.7}$$

The mean of T_M is from Eq. (B.7)

$$\text{mean}\,[T_M(\delta T_o, \delta W_R, \underline{\alpha}, \underline{\varepsilon}] = \text{mean}\,[\delta T_o] + c \cdot \text{mean}\,[\delta\Delta T_R(\delta W_R)] + \text{mean}\,[\sum_{i=1}^{M} \Delta T_i(\underline{\alpha}, \underline{\varepsilon}) \tag{B.8}$$

where the last term is given by Eq. (A.8).

The variance of T_M is from Eq. (B.7)

$$\text{var}\,[T_M(\delta T_o, \delta W_R, \underline{\alpha}, \underline{\varepsilon}] = \text{var}\,[\delta T_o] + c^2 \cdot \text{var}\,[\delta \Delta T_R(\delta W_R)]$$

$$+ c \cdot \text{cov}\,[\delta T_o, \delta \Delta T_R(\delta W_R)] + \text{var}\left[\varepsilon_1 + \sum_{i=1}^{M} \Delta T_i(\underline{\alpha}, \underline{\varepsilon})\right]$$

where the last term is given by Eq. (A.9). The covariance of the reactor flowrate and reactor inlet temperature must be evaluated because these two quantities are not independent as a Monte Carlo analysis for CRBR showed (Ref. 2).

The usual procedure for representing the balance of plant variance is to define an associated subfactor and apply it to the subchannel coolant rise, in which case,

$$f^{s}_{ij|\sigma} = 1 + \frac{1}{\Delta T_i(\underline{0},\underline{0})} \{\text{var}\,[\delta T_o] + c^2 \cdot \text{var}\,[\delta \Delta T_R(\delta W_R)]$$

$$+ c^2 \cdot \text{cov}\,[\delta T_o, \delta \Delta T_R(\delta W_R)]\}^{1/2}$$

where

i = coolant

j = balance of plant.

APPENDIX C: COMPARISON OF TWO SIGMA VALUES AS CALCULATED USING PAST AND RECOMMENDED METHODS

This Appendix makes use of a numerical example to quantify the difference between the two sigma value as calculated in past Applied Physics work (i.e. the 5-factor vertical method) and as calculated in accord with the recommendation made in the text to use the horizontal approach.

The procedure for comparison is as follows. Recall there were three basic discrepancies between past and present approaches. First, past work made use of the vertical implementation of the semistatistical method instead of the horizontal implementation recommended here. Second, in the past hot channel factors from CRBR were applied outright to other reactors without examining the validity of this transfer. Third, some of these hot channel factors were applied incorrectly. To isolate the effect of each of these differences, a numerical example is worked through three times, each time with only one of the three discrepancies present. In each case, the hot spot temperature is calculated as it would have been prior to this report and then with the source of the discrepancy removed as per this report. Finally an example is worked through with all discrepancies acting simultaneously. The numerical examples are based on the small LMR and values for hot spot subfactors and hot channel factors used in the calculation will be introduced as they are required.

C.1 Vertical versus Horizontal

The effect of using the vertical approach versus the horizontal approach is shown here through an example. Subfactor values for both cases are taken from Table II while nominal temperatures are taken from Table III. The horizontal case has already been worked through in Section 6 in Table III. Calculation via the vertical approach is shown in Table C.1. The vertical two sigma cladding midwall temperature of 1266 (°F) is 3 (°F) higher than the horizontal temperature of 1263 (°F).

C.2 CRBR Subfactors Applied to Different Reactors

In past hot spot analyses in the Applied Physics Division, CRBR uncertainty data has been applied to reactors other than CRBR to obtain two sigma temperatures. Naturally there is some question as to whether CRBR uncertainty data can adequately represent that of a different reactor. To determine this, the following simple test was performed. The small LMR subfactor data of Table II was applied via the horizontal approach to Table III nominal temperatures. The calculation is shown in Table III and yielded a value of 1263 (°F). Then CRBR subfactor data of Table 1 of Ref. 3 (which is reproduced in Table C.2) was applied via the horizontal approach to the Table III LMR nominal temperatures and yielded a value of 1282 (°F). The calculation is shown in Table C.3. The effect of using CRBR data for another reactor resulted in a 19 (°F) overestimate for cladding temperature.

C.3 Uncertainty Data Used Incorrectly

This subsection outlines errors that have been made in the past in the application of uncertainty data. The effect of these errors on hot spot temperature is gauged below by computing a two sigma value with the errors

present and then correcting the errors, recomputing the two sigma value and then comparing the two results.

Past errors center around the use of hot channel factor values pulled from Table 1 of Ref. 3 and input to NIFD for a two sigma cladding midwall temperature. For the sake of completeness, calculation of the Ref. 3 Table 1 hot channel factors from the subfactors in the same table via the vertical approach is given below.

$$f_{coolant} = 1.03\ (1.05)\ 1.08\ \left\{1 + \frac{2}{3}\left[(0.02)^2 + (0.04)^2 + (0.06)^2 + (0.01)^2 + (0.01)^2 + (0.028)^2 + (0.01)^2\right]^{1/2}\right\} = 1.232$$

$$f_{film} = 1.035\ (1.7)\ \left\{1 + \frac{2}{3}\left[(0.12)^2 + (0.15)^2\right]^{1/2}\right\} = 1.985$$

$$f_{cladding} = 1.7\ \left\{1 + \frac{2}{3}\left[(0.15)^2 + (0.12)^2\right]^{1/2}\right\} = 1.918$$

$$f_{heat\ flux} = 1.03\ \left\{1 + \frac{2}{3}\left[(0.065)^2 + (0.035)^2\right]^{1/2}\right\} = 1.081$$

Note that in Table 1 of Ref. 3, the two and three sigma hot channel factors for cladding temperature rise for cladding midwall two sigma temperature are missing. The value is calculated above, however.

The first incorrect use of uncertainty data centers on the extraction of hot channel factor values from Table 1 of Ref. 3. The proper hot channel factor values for cladding midwall are shown above. The set of values, however, that has been used in the Division and is said to have been taken from CRBR Table 1 of Ref. 3 differs as shown below.

Two Sigma Cladding Midwall Hot Channel Factors

Hot Channel Factor	Table 1 of Ref. 3	Past Work (Page 5 of Ref. 4)
$f_{coolant}$	1.232	1.232
f_{film}	1.986	1.168
$f_{cladding}$	1.918	1.128
$f_{heat\ flux}$	1.081	1.081

Clearly the two sigma cladding and film hot channel factor values listed above do not agree with the corresponding entries in Table 1 of Ref. 3. A closer look shows that the AP values are actually CRBR fuel centerline values taken from Table 1 of Ref. 3. Hence, error one: film and cladding hot channel factors derived for CRBR fuel centerline temperature have been applied to cladding midwall temperature calculations.

The second error involves the treatment of uncertainty in physics methods and control rod position. In Table 1 of Ref. 3 these uncertainties are not included as subfactors since they were applied to peaking factors. Since the hot channel factor values given at the bottom of the table are derived from the subfactors above the hot channel factor, values given do not include the effect of physics methods and control rod position uncertainty. To compute hot channel factors from Table 1 that include these uncertainties we note from the Table 1 footnote that these effects contribute a 4% error to coolant enthalpy rise and 5% error to heat flux. The new hot channel factors are then

$$f_{coolant} = 1.232 \cdot 1.04 = 1.281$$

$$f_{film} = 1.985$$

$$f_{cladding} = 1.918$$

$$f_{heat\ flux} = 1.081 \cdot 1.05 = 1.135$$

These values will be used in the calculation given at the end of this subsection.

The third error deals with fuel centerline temperature. The hot channel factor value for fuel temperature rise is said to be two sigma and taken from CRBR. However, looking at Table 1 of Ref. 3, the value is a three sigma quantity. It can be converted to two sigma by multiplication by two-thirds.

To quantify the affect of the first two errors discussed above, the small LMR cladding midwall temperature is computed via the vertical method twice, once with the errors intact and then with the errors corrected. The calculations are shown in Table C.4 and C.5, respectively. With past errors the cladding midwall temperature is 1247 (°F) which is 28 (°F) less than the 1275 (°F) value gotten when the errors are corrected.

C.4 Net Effect

Having looked individually at the effect of the above items, they are now combined to demonstrate their simultaneous effect. Operating on the nominal temperatures given in Table III with the semistatistical vertical approach and the hot channel factor values of Ref. 4, which contain the errors already discussed in Subsection C.3, yields a cladding midwall temperature of 1247 (°F). This value represents the temperature gotten when past methods are applied. The calculation appears in Table C.4 and is identical to the calculation of Ref. 4. Now the corresponding value computed using the procedure recommended in the text is 1263 (°F) and the calculation is shown in Table III. This was obtained using the semistatistical horizontal approach and the selected hot spot subfactors of Section 6. Therefore, the net effect of past errors is a 16 (°F) underestimate of the cladding two sigma temperature.

TABLE C.1 Small LMR Two Sigma Cladding Temperature Via Semistatistical Vertical Method

Nominal Temperatures (°F)

$T_{in} = 850$

$\Delta T_{coolant} = 309$

$\Delta T_{film} = 7$

$\Delta T_{cladding} = 6$

Hot Channel Factors (2σ)

$$f_{coolant} = 1.06\ (1.02)\ 1.02\ (1.03)\ \left[1 + \frac{2}{3}\ (0.52^2 + 0.02^2 + 0.14^2 + 0.05^2 + 0.058^2 + 0.01^2 + 0.013^2)^{1/2}\right] = 1.265$$

$$f_{film} = 1.06\ (1.02)\ 1.006\ (1.14)\ 1.8\ \left[1 + \frac{2}{3}\ (0.052^2 + 0.02^2 + 0.005^2 + 0.12^2 + 0.174^2)^{1/2}\right] = 2.557$$

$$f_{cladding} = 1.06\ (1.02)\ 1.14\ (0.8)\ 1.05\ \left[1 + \frac{2}{3}\ (0.052^2 + 0.02^2 + 0.174^2)^{1/2}\right] = 1.161$$

Cladding Midwall Temperature (2σ)

$$T^{2\sigma} = 850 + 309\ (1.265) + 7\ (2.557) + 6\ (1.161) = 1266\ (°F)$$

TABLE C.2 CRBR Fuel Assembly Cladding Hot Spot Subfactors (Ref. 14)

	Coolant	Film	Cladding
Direct			
Power level measurement and control system dead band	1.03		
Inlet flow maldistribution	1.05		
Assembly flow maldistribution calculational uncertainties	1.08	1.035	
Cladding circumferential temperature variation		1.7	1.7
Physics analysis calculational methods and control rod effects	1.04	1.05	1.05
Statistical (3 σ)			
Inlet temperature variation	1.02		
Reactor ΔT variation	1.04		
Nuclear data	1.06		
Fissile fuel maldistribution	1.01		
Wire wrap orientation	1.01		
Subchannel flow area	1.028		
Film heat transfer coefficient		1.12	
Pellet-cladding eccentricity		1.15	1.15
Cladding thickness and conductivity			1.12
Coolant properties	1.01		

TABLE C.3 Calculation of Two Sigma Cladding Midwall Temperature Using Horizontal Method and Small LMR Nominal Temperatures and CRBR Subfactors

	Inlet T	Coolant ΔT	Film ΔT	Cladding MW ΔT	Total
1. Nominal Temperatures (°F)	850	309	7	6	1172
2. 0σ Temperatures (°F)	850	375.4 (= 309*1.03*1.05* 1.08*1.04)	12.9 (= 7.0*1.035* 1.7*1.05)	10.7 (= 6.1*7.1*1.05)	
3. 3σ Temperature Uncertainties (°F)					
Inlet temperature variation		6.2			6.2
Reactor ΔT variation		12.4			12.4
Nuclear data		18.5			18.5
Fissile fuel maldistribution		3.1			3.1
Wire wrap orientation		3.1			3.1
Subchannel flow area		8.7			8.7
Film heat transfer coefficient			0.8		0.8
Pellet cladding eccentricity			1.1	0.9	2.0
Cladding thickness and conductivity				0.7	0.7
Coolant Properties		3.1			3.1
					$[\Sigma(3\sigma_i)^2]^{1/2} = 25.4$
4. 2σ Peak Cladding Midwall Temperature (°F)					

$$T^{2\sigma}_{clad} = 850 + 16 + (375.4 + 12.9 + 10.7) + \frac{2}{3}(25) = 1282$$

TABLE C.4 Example of Applying Uncertainty Data Incorrectly Via Vertical Method

Nominal Temperatures (°F)

$T_{in} = 850$

$\Delta T_{coolant} = 309$

$\Delta T_{film} = 7$

$\Delta T_{cladding} = 6$

Hot Channel Factors (2σ, Ref. 4)

$f_{coolant} = 1.232$

$f_{film} = 1.168$

$f_{cladding} = 1.128$

$f_{heat\ flux} = 1.081$

Cladding Midwall Temperature (2σ)

$$T^{2\sigma} = 850 + 309\ (1.232) + 7\ (1.168)\ 1.081 + 6\ (1.128)\ 1.081$$

$$= 1247\ (°F)$$

TABLE C.5 Example of Applying Uncertainty Data Correctly Via Vertical Method

Nominal Temperatures (°F)

$T_{in} = 850$

$\Delta T_{coolant} = 309$

$\Delta T_{film} = 7$

$\Delta T_{cladding} = 6$

Hot Channel Factors (2σ, Ref. 3)

$f_{coolant} = 1.281$

$f_{film} = 1.985$

$f_{cladding} = 1.918$

$f_{heat\ flux} = 1.135$

Cladding Midwall Temperature (2σ)

$$T^{2\sigma} = 850 + 309\ (1.281) + 7\ (1.985)\ 1.135 + 6\ (1.918)\ 1.135$$

$$= 1275\ (°F)$$

APPENDIX D: CALCULATION OF SUBCHANNEL FLOW AREA HOT SPOT SUBFACTOR

This appendix shows how the value of the small LMR subchannel flow area subfactor can be deduced from the work done for CRBR.

We begin by assuming the following four items are known: the value of the CRBR subchannel flow area hot spot factor f^s_{CRBR}; the value of the CRBR nominal channel area $A_{n,CRBR}$; the value of the desired channel area $A_{n,desired}$; and that the standard deviation in the desired channel area is the same as CRBR. From Ref. 7 the effect of channel area on coolant temperature rise is

$$\frac{\Delta T_h}{\Delta T_n} = \left(\frac{A_n}{A_h}\right)^{5/3} \tag{D.1}$$

where

A_n = nominal subchannel area

A_h = perturbed subchannel area

ΔT_n = nominal temperature rise with area A_n

ΔT_h = temperature rise with area A_h.

Now write

$$A_h = A_n - \epsilon \tag{D.2}$$

where ϵ represents the error in area and is a zero mean random variable with standard deviation $\bar{\sigma}$. Then, from the definition of the statistical hot spot subfactor in Appendix A, the subchannel area hot spot subfactor is

$$f^s(\bar{\sigma}) = \left(\frac{A_n}{A_n - \bar{\sigma}}\right)^{5/3} \tag{D.3}$$

The standard deviation of the subchannel area uncertainty in CRBR is gotten by solving Eq. D.3 for $\bar{\sigma}$ where

$$f^s(\bar{\sigma}) = f^s_{CRBR}$$

$$A_n = A_{n,CRBR}$$

Then the statistical hot spot factor for the desired geometry, based on CRBR area uncertainty is gotten by solving Eq. D.3 for $f^s(\bar{\sigma})$ where

$\bar{\sigma}$= standard deviation of area in CRBR

$A_n = A_{n,desired}$